

## PAPER

# An Opening-Snap Heart Sound-Aware DGMC- $L_{1,2}$ -Based Multi-Heart Disease Prediction Using ECG and PCG

Dakshayani Himabindu  
 Damineni<sup>1</sup>(✉), CH.  
 Srilakshmi<sup>2</sup>, Jakkula  
 Sravanthi<sup>1</sup>, B. Sivalakshmi<sup>3</sup>,  
 Satish Kumar Mirtipati<sup>4</sup>,  
 Prasanthi Yavanamandha<sup>5</sup>

<sup>1</sup>Department of IT, VNRVJIEET,  
 Hyderabad, Telangana, India

<sup>2</sup>Department of CSE-IOT, CBIT,  
 Hyderabad, Telangana, India

<sup>3</sup>Department of Information  
 Technology & MCA, Vignan's  
 Institute of Engineering  
 for Women (Autonomous),  
 Kappujagarajupeta, Andhra  
 Pradesh, India

<sup>4</sup>Department of CSE,  
 CENTURION University  
 of Technology and  
 Management, Andhra  
 Pradesh, India

<sup>5</sup>Department of CSE – AIML  
 & IOT, VNRVJIEET, Hyderabad,  
 Telangana, India

[dakshayani.himabindu@gmail.com](mailto:dakshayani.himabindu@gmail.com)

**ABSTRACT**

Recently, multi-heart disease diagnosis has become a popular research domain. Yet the traditional systems were ineffective due to the limited signal-processing approaches. Therefore, a deep generalized extreme value mish convolutional neural network with  $L_{1,2}$  regularization (DGMC- $L_{1,2}$ )-based multi-heart disease classification is implemented in this paper using electrocardiogram (ECG) and phonocardiogram (PCG). Primarily, the ECG and PCG are gathered and then preprocessed. After preprocessing, the peak waves are identified using the discrete cross-wavelet transform (DCWT). In the same way, the Osborn wave (OW) and opening snap (OS) are predicted from the ECG and PCG, respectively, using fuzzy exponential-decay-riseton inference system (FEDRIS), followed by wave interval segmentation. Furthermore, the dendrogram with a scatter plot is generated, and then the features are extracted. In addition, the peak localized ECG and PCG are fused together. Subsequently, the subsequent derivatives are estimated, and then a bivariate correlation matrix is created. Then, the feature extraction is done, followed by dimensionality reduction. Here, the dimensionalities of the features are reduced using log-linear scaling<sup>2</sup>—Principal Component Analysis (LS<sup>2</sup>-PCA) and then fed into the proposed DGMC- $L_{1,2}$ , which effectively predicts multi-heart diseases. Thus, the experimental results proved that the proposed work had high supremacy with an accuracy of 98.99%.

**KEYWORDS**

multi-heart disease classification, electrocardiogram (ECG), phonocardiogram (PCG), opening snap (OS), deep generalized extreme value mish convolutional neural network with  $L_{1,2}$  regularization (DGMC- $L_{1,2}$ ), fuzzy exponential-decay-riseton inference system (FEDRIS), dendrogram and Osborn wave (OW)

**1 INTRODUCTION**

Cardiovascular diseases (CVDs), with heart disease being a component, stand as the cause of death across the globe [1]. They lead to around 17.9 million deaths each year, making up 32% of all deaths [2]. Low- and middle-income countries experience

Damineni, D.H., Srilakshmi, CH., Sravanthi, J., Sivalakshmi, B., Mirtipati, S.K., Yavanamandha, P. (2024). An Opening-Snap Heart Sound-Aware DGMC- $L_{1,2}$ -Based Multi-Heart Disease Prediction Using ECG and PCG. *International Journal of Online and Biomedical Engineering (iJOE)*, 20(14), pp. 85–101. <https://doi.org/10.3991/ijoe.v20i14.51371>

Article submitted 2024-07-25. Revision uploaded 2024-09-03. Final acceptance 2024-09-03.

© 2024 by the authors of this article. Published under CC-BY.

over 75% of these fatalities, mainly due to limited healthcare access [3] [4]. The prevalence of heart disease is rising globally due to aging populations, sedentary lifestyles, poor diets, and increasing obesity rates.

Detecting heart disease early is essential, as it results in lessening disability, cutting down on expenses, and recognizing issues such as blood pressure. Clogged arteries in their initial phases allow for timely actions that can halt the progression of diseases and lessen complications. Artificial intelligence (AI) is becoming increasingly crucial in spotting problems and providing treatment [5]. AI boosts the accuracy of analysis, identifies risk factors by analyzing amounts of data, and enhances the precision of diagnoses in interpreting imaging scans and Electrocardiogram (ECG) results. Wearable devices powered by AI enable continuous monitoring of heart health from a distance, allowing the detection of potential concerns in real time.

Electrocardiogram monitors the heart's electrical activity and detects arrhythmias and heart attacks; we need expert interpretation and are limited in assessing structural heart issues [6]; Phonocardiogram (PCG) helps to record heart sounds to diagnose murmurs and valve disorders, PCG is sensitive to noise and cannot detect electrical abnormalities [7]. In clinical settings, PCG is used as short-term monitoring and relies heavily on human expertise so that we can lead to diagnostic errors. In low-resource regions, we cannot access advanced ECG and PCG technology. These study gaps can be addressed by applying AI and machine learning (ML), which helps enhance the accuracy and interpretation of ECG and PCG data [8]. We can use wearable devices for real-time heart monitoring outside clinical environments and combine ECG and PCG in multimodal systems for a more comprehensive assessment of cardiovascular health [9] [10].

## 2 LITERATURE SURVEY

[11] propounded convolutional neural network (CNN)-based accurate cardiovascular disease recognition using PCG. Primarily, the PCG was subjected to pre-processing and feature extraction. Then, the features were fed into the CNN to classify the HD efficiently. However, this had information loss due to the energy threshold-based peak localization.

[12] incorporated ECG-based heart disease prediction using a hybrid feature selection approach. Here, a multi-module neural network was introduced to effectively classify whether the individual was affected by heart disease or not. However, this method only concentrated on P, Q, R, S, and T, causing poor outcomes.

[13] introduced automatic prediction of heart valve diseases using PCG signals. Here, the ensemble-ML classifier was introduced to classify the HD. This technique had maximum accuracy. However, it failed to perform pre-processing, causing a high misclassification rate.

[14] developed two-stage classification-based coronary artery disease detection using PCG. Initially, the fused features were inputted to the K-nearest-neighbor (KNN) and support vector machine (SVM), where various types of HD were obtained. Yet, it had computational complexity due to the high feature dimensions.

[15] established PCG-based automatic detection of heart valve diseases using the multiclass composite classifier. Initially, the crucial features were extracted and then fed into the multiclass composite classifier, thus predicting the HD significantly. Nevertheless, it was ineffective due to the inadequate features.

Recently, techniques such as the hidden Markov model (HMM), SVM, and CNN have been introduced to perform multi-head depth wise convolution (MHDC) [9] [10]. However, the traditional works were insignificant owing to the limited features.

To bridge these gaps, this paper introduces a DGMC-L<sub>1,2</sub>-based approach for multi-heart disease classification, utilizing both ECG and PCG signals. This method stands out from previous work by highlighting the significance of OS sound in heart disease diagnosis, a factor often neglected. The proposed FEDRIS technique enhances prognosis by accurately detecting OS sounds in PCG signals, coupled with amplitude threshold-based peak localization to improve diagnostic accuracy. Additionally, LS<sub>2</sub>-PCA is employed for dimensionality reduction, reducing the computational burden caused by high-dimensional features, while OW is leveraged to refine MHDC results, offering a more thorough and efficient solution for heart disease classification.

### 3 PROPOSED SYSTEM FOR DGMC-L<sub>1,2</sub>-BASED MHDC

The proposed DGMC-L<sub>1,2</sub>-based MHDC is implemented in this paper using ECG and PCG. The proposed work's architecture is given in Figure 1.

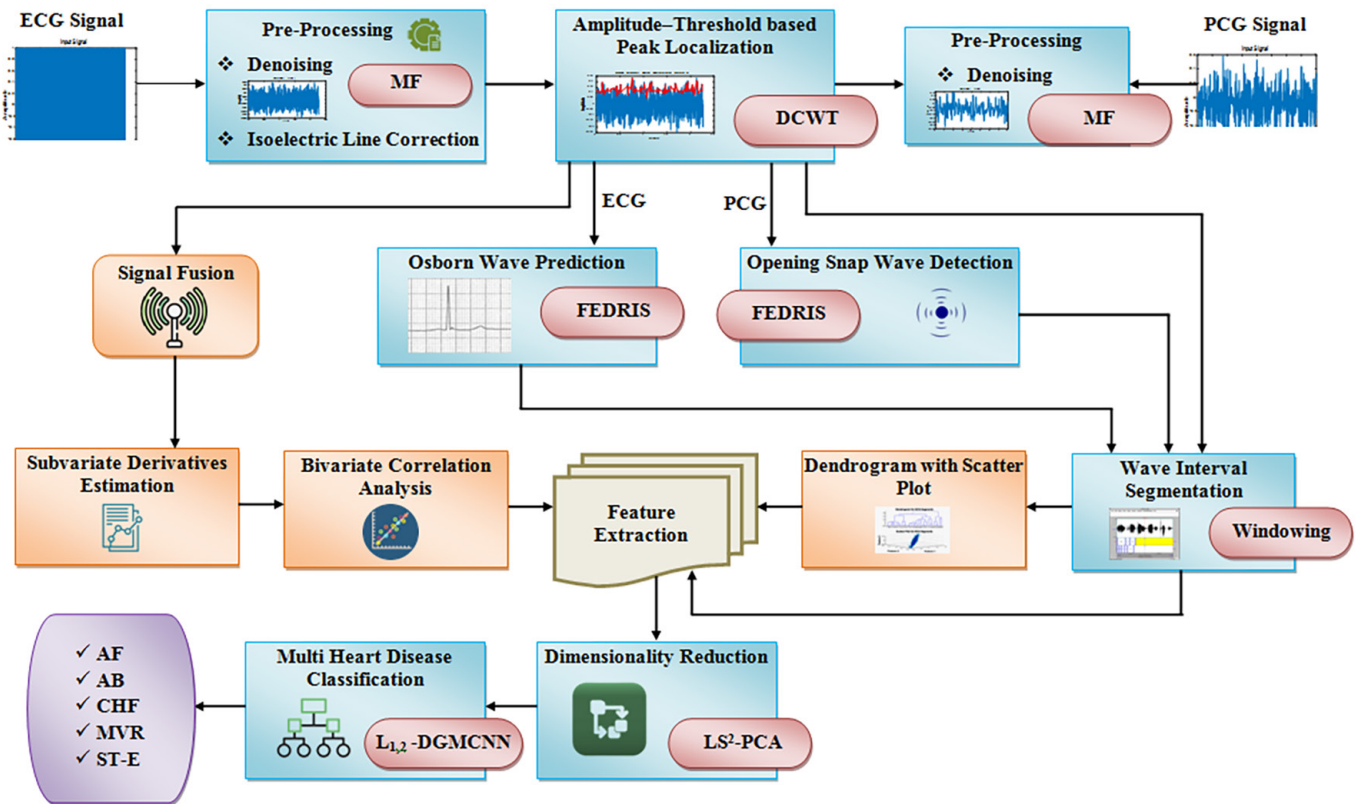


Fig. 1. The proposed work's architecture

#### 3.1 Electrocardiogram and phonocardiogram

Primarily, the input ECG and PCG are gathered to implement the proposed MHDC framework.

$$(\phi_g^{ECG}, \gamma_n^{PCG}) = \sum_{g,n} \|\phi_1^{ECG}, \phi_g^{ECG} \dots \phi_G^{ECG}\|, \|\gamma_1^{PCG}, \gamma_n^{PCG} \dots \gamma_N^{PCG}\| \quad (1)$$

Where,  $g = 1$  to  $G$  depicts the number of ECG signals  $\phi_g^{ECG}$  and  $n = 1, 2, \dots, N$  indicates the number of PCG signals  $\gamma_n^{PCG}$ .

### 3.2 Electrocardiogram pre-processing

Here, the  $\phi_g^{ECG}$  is pre-processed under denoising and isoelectric line correction, The noises in the  $\phi_g^{ECG}$  are eradicated using a Median Filter (MF). The MF operation ( $M_\theta$ ) is given as,

$$M_\theta(\zeta, \nu) = \underset{(\psi_1, \psi_2) \in \phi_g^{ECG}}{\text{median}} * \{\phi_g^{ECG}(\psi_1, \psi_2)\} \tag{2}$$

Here,  $\zeta$  and  $\nu$  denote the horizontal axis and vertical axis, respectively, and  $\psi_1$  and  $\psi_2$  depict the neighborhood entries. The filtered ECG is mentioned as  $\beta_g^{ECG}$ .

Next, the isoelectric line in  $\beta_g^{ECG}$  is corrected to improve the model outcomes. Finally, the pre-processed ECG ( $\wp_t$ ) is defined below,

$$\wp_t = (\wp_{t1}, \wp_{t2}, \dots, \wp_{tT}) \text{ Where } t = 1 \text{ to } T \tag{3}$$

where,  $T$  denotes the number of  $\wp_t$ .

### 3.3 Phonocardiogram pre-processing

Likewise, the  $\gamma_n^{PCG}$  is pre-processed under noise removal based on MF. Here, the noises in  $\gamma_n^{PCG}$  are eliminated using MF. Thus, the  $r = 1, 2, \dots, R$  number of pre-processed PCG is shown as ( $O_r$ ).

### 3.4 Amplitude threshold-based peak localization

Afterward, the  $\wp_t$  and  $O_r$  are subjected to the amplitude threshold-based peak localization. The proposed method employs the DCWT to localize the peak waves from the  $\wp_t$  and  $O_r$ . The discrete wavelet transform (DWT) is employed because it has high computational efficiency. However, the DWT had information loss during decomposition. Therefore, the cross-entropy decomposition is employed to preserve the significant details.

Here, the threshold is determined by considering the amplitude of the signal. The DWT of the  $\wp_t$  and  $O_r$  is determined by passing through the series of filters. Initially, the  $\wp_t$  and  $O_r$  are passed through the low-pass filter ( $\mathfrak{R}^\circ$ ),

$$Lw(y) = (\wp_t, O_r) * \mathfrak{R}^\circ | y | \rightarrow \sum_{s=-\infty}^{\infty} (\wp_t, O_r) \cdot s \mathfrak{R}^\circ (y - s) \tag{4}$$

Where,  $Lw$  denotes the DWT,  $y$  indicates the level count, and  $s$  denotes the shift parameter.

Next, the  $\wp_t$  and  $O_r$  are decomposed using the cross-entropy decomposition ( $DV$ ),

$$DV^{X||Y}(\wp_t, O_r) = W_{X(\wp_t, O_r)} [-\log Y(\wp_t, O_r)] \tag{5}$$

Here,  $X$  and  $Y$  depicts the distribution parameters and  $W$  illustrates the entropy function.

Subsequently, the low-pass filtered result and decomposed output are inputted to the new low-pass filter and new decomposition as,

$$LW_{low}(y) = \sum_{s=-\infty}^{\infty} (\wp_t, O_r) \cdot s\Re^{\circ}(2y - s) \tag{6}$$

$$LW_{high}(y) = \sum_{s=-\infty}^{\infty} (\wp_t, O_r) \cdot sD\nabla^{X||Y}(2y - s) \tag{7}$$

Next, the sub-sampling operator is calculated and then applied in the low-pass filter and decomposition operation as,

$$(LW \downarrow s)[y] = LW(sy) \tag{8}$$

$$LW_{low} = (\wp_t, O_r) \times \Re^{\circ} \downarrow 2 \tag{9}$$

$$LW_{high} = (\wp_t, O_r) \times D\nabla \downarrow 2 \tag{10}$$

Finally, the heart waves, such as  $P(p_{\theta})$ ,  $Q(q_{\theta})$ ,  $R(r_{\theta})$ ,  $S(s_{\theta})$ , and  $T(t_{\theta})$  are extracted from the ECG. Likewise, the heart sounds such as  $S1(\chi_1)$ ,  $S2(\chi_2)$ ,  $S3(\chi_3)$ , and  $S4(\chi_4)$ , and murmurs ( $\mu r$ ) are extracted from the PCG.

Thus, the extracted heart waves ( $H\alpha$ ) and heart sounds ( $H\delta$ ) are shown below,

$$H\alpha \rightarrow \{p_{\theta}, q_{\theta}, r_{\theta}, s_{\theta}, t_{\theta}\} \tag{11}$$

$$H\delta \rightarrow \{\chi_1, \chi_2, \chi_3, \chi_4, \mu r\} \tag{12}$$

Then, the OW and OS are predicted from the  $H\alpha$  and  $H\delta$ , respectively.

### 3.5 Osborn wave prediction

Next, the OW is predicted from the  $H\alpha$  using FEDRIS. The fuzzy inference system (FIS) is selected because it provides optimal reasoning. Yet, it had tuning difficulties due to the traditional membership function. Therefore, the exponential decay rise-ton (EDR) membership function is introduced to improve the prediction outcomes.

Initially, the fuzzy rules ( $\Im$ ule) are framed to predict the OW from the  $H\alpha$ .

$$\Im$$
ule  $\rightarrow \{IF(q_{\theta}, r_{\theta}, s_{\theta}) \downarrow \& \& (s_{\theta}, t_{\theta}) \mapsto == 20 \text{ to } 120 \text{ ms} \text{ THEN } \alpha s_{wave} \tag{13}$

The OW ( $\alpha s_{wave}$ ) is predicted by considering the point at which the QRS complex finishes and the ST segment begins. Also,  $\alpha s_{wave}$  occurs during the time interval of 20 to 120ms.

Then, the proposed work introduces the EDR membership function ( $Mem^{\Omega}$ ).

$$Mem^{\Omega} = \begin{cases} 1 - (\exp^{-a(H\alpha - b)})^2, & IF(a < H\alpha \leq b) \\ 0, & IF(H\alpha \neq f) \\ 1, & IF(H\alpha = f) \end{cases} \tag{14}$$

Where,  $a$  and  $b$  indicate the constant parameters and  $f$  illustrates the mid-value. Moreover, the crisp data is converted into fuzzy data in the fuzzification unit. Similarly, the fuzzy data is transformed into crisp data in the defuzzification unit. The pseudo-code of the proposed FEDRIS is illustrated below,

**Input:** Heart waves  $H\alpha$   
**Output:** OW prediction  
**Begin**  
    **Initialize**  $\alpha_{S_{wave}}$ ,  $a$  and  $b$   
    **Generate** fuzzy rules,  
     $\text{Rule} \rightarrow \{IF(q_{\theta}, r_{\theta}, s_{\theta}) \downarrow \& \& (s_{\theta}, t_{\theta}) \mapsto == 20 \text{ to } 120 \text{ ms THEN } \alpha_{S_{wave}}\}$   
    **Apply** EDR membership function ( $Mem^{\Omega}$ )  

$$Mem^{\Omega} = \begin{cases} 1 - (\exp^{-a(H\alpha - b)})^2, & IF(a < H\alpha \leq b) \\ 0, & IF(H\alpha \neq f) \\ 1, & IF(H\alpha = f) \end{cases}$$
  
    **Convert** fuzzy data  
    **Execute** defuzzification  
**Return**  $\alpha_{S_{wave}}$   
**End**

### 3.6 Opening snap prediction

Likewise, the OS is predicted from  $H\delta$  using FEDRIS. The steps involved in the proposed FEDRIS are already discussed in the section 3.5. Moreover, the fuzzy rules are framed as,

$$\text{Rule} \rightarrow \{IF(\chi_2 \downarrow) == 40 \text{ to } 120 \text{ ms THEN } \vartheta_{S_{sound}}^{\xi}\} \tag{15}$$

Here, the OS ( $\vartheta_{S_{sound}}^{\xi}$ ) is predicted by considering the point at which the S2 finishes. Moreover,  $\vartheta_{S_{sound}}^{\xi}$  occurs during the time interval of 40 to 120ms.

### 3.7 Wave interval segmentation

Next, the  $H\alpha$ ,  $H\delta$ ,  $\alpha_{S_{wave}}$  and  $\vartheta_{S_{sound}}^{\xi}$  are subjected to the wave interval segmentation based on windowing. Here, the wave intervals, such as P-R, Q-T, P-OS, and OS-T are segmented from the  $H\alpha$  and  $\alpha_{S_{wave}}$ . Likewise, the sound intervals such as S1-S2, S1-OS, and OS-S4 are segmented from the  $H\delta$  and  $\vartheta_{S_{sound}}^{\xi}$ . The sliding window ( $Sg$ ) is used to estimate the number of waves in a particular time interval. The segmented wave intervals ( $\omega\alpha\nu\varepsilon_{int}$ ) and sound intervals ( $\delta\mu\eta\theta_{int}$ ) are shown below,

$$Sg = (\omega\alpha\nu\varepsilon_{int}, \delta\mu\eta\theta_{int}) \tag{16}$$

Next, the dendrogram with a scatter plot is generated in the  $\omega\alpha\nu\varepsilon_{int}$  and  $\delta\mu\eta\theta_{int}$ .



### 3.8 Dendrogram with scatter plot

Furthermore, the dendrogram is created from the  $\omega\alpha\nu\varepsilon_{int}$  and  $\delta\sigma\mu\eta\partial_{int}$ . Generally, a dendrogram is used to represent the relationship among a group of signal entities. Next, the scatter plot is introduced to perform color mapping. Finally, the generated dendrogram with a scatter plot ( $DS_{plot}$ ) provides more informative details about the signal waves.

### 3.9 Signal fusion

Likewise, the peak localized ECG and PCG are fused together by mapping the QRS complex and S1-S2 point. The fused signals are mentioned as ( $N_{fused}$ ).

### 3.10 Subvariate derivatives estimation

Next, the subvariate derivatives such as first-order ( $\lambda_{first}$ ), second-order ( $\zeta_{second}$ ), and third-order ( $\beta_{third}$ ) are estimated from  $N_{fused}$  by using the amplitude and time-frequency. The estimated subvariate derivatives ( $Sub_v$ ) are illustrated as,

$$Sub_v = \langle \lambda_{first}, \zeta_{second}, \beta_{third} \rangle \quad (17)$$

The derivative form of the signals helps to detect the heart rate of the patients accurately.

### 3.11 Bivariate correlation analysis

Then, the bivariate correlation matrix is generated from  $Sub_v$  to analyze the relationship among the various signal entities. The bivariate correlation matrix ( $B\Xi$ ) is created as,

$$B\Xi = \frac{Sub_v \cdot \sum (\lambda_{first}, \zeta_{second}, \beta_{third} - mn)}{\sqrt{Sub_v \cdot \sum (\lambda_{first}, \zeta_{second}, \beta_{third} - mn)^2}} \quad (18)$$

Where,  $mn$  depicts the mean value.

### 3.12 Feature extraction

Here, the  $\omega\alpha\nu\varepsilon_{int}$ ,  $\delta\sigma\mu\eta\partial_{int}$ ,  $DS_{plot}$  and  $B\Xi$  are inputted to the feature extraction. The crucial features such as signal\_range, curved, bandwidth for PCG signal, frequency bands, form, and maximum cluster are extracted. The extracted features are shown as ( $M_\Phi$ ).

### 3.13 Dimensionality reduction

Next, the dimensionalities of  $M_\Phi$  are reduced using the log-linear scaling<sup>2</sup>-LS<sup>2</sup>-PCA. The PCA efficiently reduces the feature space without information loss. Yet, it had

computational complexity due to the traditional standardization. So, the log-linear scaling<sup>2</sup> normalization (*Std*) is used to perform standardization.

$$Std = \log(M_\phi) * \frac{|M_\phi - \min(M_\phi)|}{|\max(M_\phi) - \min(M_\phi)|} \tag{19}$$

Thereafter, the covariance matrix ( $K^\circ$ ) is created as,

$$K^\circ = Std \cdot \frac{1}{V-1} \cdot \sum_{\phi=1}^V \begin{bmatrix} (M_1, M_1) & (M_1, M_2) \\ (M_2, M_1) & (M_2, M_2) \end{bmatrix} \tag{20}$$

Where,  $\Phi = 1$  to  $V$  depicts the number of  $M_\phi$ . Also, the eigenvectors (*Eig*) and eigenvalues (*eg*) are determined from the  $K^\circ$ ,

$$K^\circ \times eg = Eig * eg \tag{21}$$

Subsequently, the eigenvector with the highest eigenvalue is assumed as the principal component, which reduces the dimensionality of the features. The dimensionality-reduced features are illustrated as ( $\partial im_j$ ).

### 3.14 Multi-heart disease classification

Next, the  $\partial im_j$  is fed into the proposed DGMC- $L_{1,2}$  to classify the five types of HD. The deep convolutional neural network (DCNN) efficiently captures the complex features. Yet it had overfitting issues and low learning efficiency. Therefore, the  $L_{1,2}$  norm-regularization and generalized extreme value mish (GM) activation functions are introduced to improve the classifier performance. The structure of the DGMC- $L_{1,2}$  is shown in Figure 2.

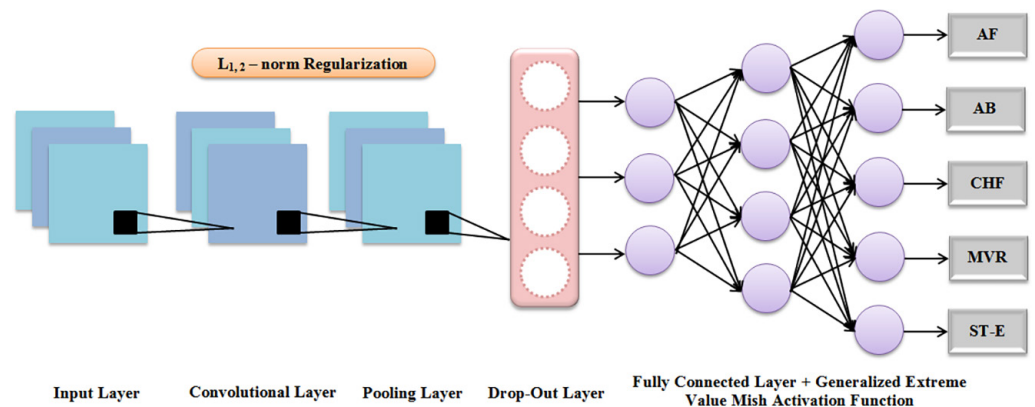


Fig. 2. The pictorial depiction of the proposed DGMC- $L_{1,2}$

Primarily, the input layer holds  $\partial im_j$  and then transfers them to the further network layers.

Next, the convolutional layer is used to extract the features from the  $\partial im_j$ .

Then, the ratio of the feature maps is reduced in the pooling layer (*Po*).

Afterward, the  $L_{1,2}$  norm-regularization is used to initialize the weight parameter (*Wt*),



$$Wt = \|mx(Po_l)\|_{2,1} = \sum_{o=1}^O \sqrt{\sum_{p=1}^P mx_{o,p}^2(Po_l)} = \sum_{o=1}^O \|mx^o(Po_l)\|_2 \quad (22)$$

Where,  $mx$  indicates the regularization matrix, and  $O$  and  $P$  depict the norm parameters.

Furthermore, the dropout layer is used to eliminate the inconsistent features. Next, the fully-connected layer ( $Fu_{connect}$ ) is equated as,

$$Fu_{connect} = (gmh * |Wt \cdot \partial im_j|) + Bis \quad (23)$$

Here,  $Bis$  indicates the bias and  $gmh$  illustrates the Gated Modification (GM) activation function, which is given below,

$$gmh(\partial im_j | l_1 w_1, d_1) = \begin{cases} MSh + \exp\left(-\exp\left(\frac{\partial im_j - w_1}{d_1}\right)\right), & IF(l_1 = 0) \\ MSh + \exp\left(-\left(1 + l_1 \left(\frac{\partial im_j - w_1}{d_1}\right)^{-\frac{1}{l_1}}\right)\right), & IF(l_1 \neq 0) \end{cases} \quad (24)$$

$$Msh = \partial im_j \tanh(\log(1 + \exp^{\partial im_j})) \quad (25)$$

Finally, the output layer ( $Ol$ ) classifies the HD into five types, namely atrial fibrillation (AF), atrio-ventricular block (AB), congestive heart failure (CHF), mitral valve regurgitation (MVR), and ST-elevation (ST-E). The pseudo-code of the proposed DGMC-L<sub>1,2</sub> is given further,

**Input:** Dimensionality reduced features  $\partial im_j$

**Output:** Classified output  $Ol$

**Begin**

**Initialize**  $mx, Bis, gmh, Wt$  and  $Msh$

**Perform** convolutional layer

**Initialize** weight  $Wt = \|mx\|_{2,1} = \sum_{o=1}^O \sqrt{\sum_{p=1}^P mx_{o,p}^2} = \sum_{o=1}^O \|mx^o\|_2$

**Execute** fully-connected layer,

$$Fu_{connect} = (gmh * |Wt \cdot \partial im_j|) + Bis$$

**Apply** GM activation function  $gmh$

**Return** ( $Ol$ )

**End**

Thus, the research framework effectively enhances the patient's lifestyle via precise multi-head depth wise convolution.

## 4 RESULTS

The performance of the proposed methodology is validated to showcase the model's efficacy. The proposed system is implemented in the Python platform.

### 4.1 Dataset description

The proposed work is assessed by using the PhysioNet dataset, which is mentioned in the reference section. Here, the ECG and PCG signals are manually gathered from the various sources in the PhysioNet. From the whole data, 80% of the data is employed for training, and the remaining data is used for testing. The image results are depicted in Table 1.

Table 1. Sample image results

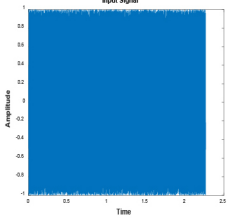
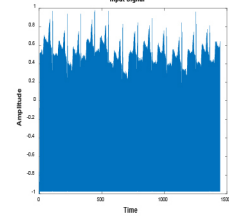
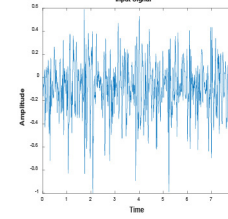
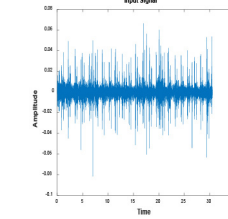
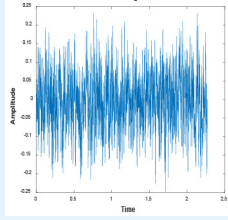
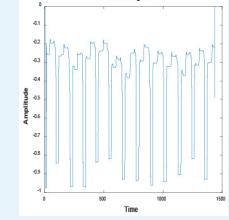
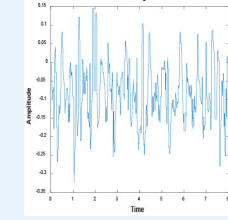
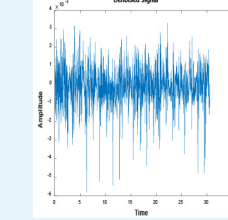
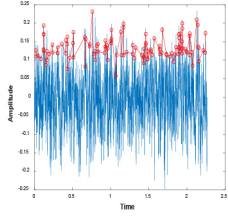
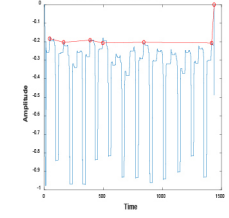
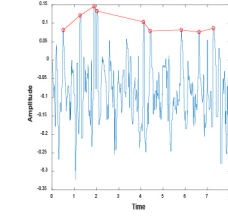
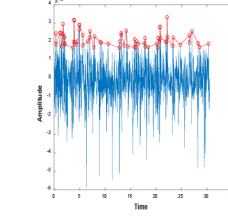
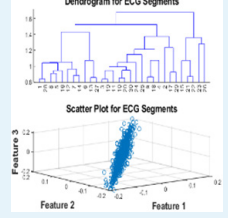
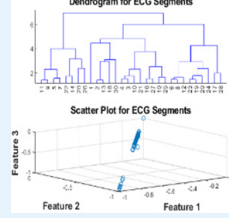
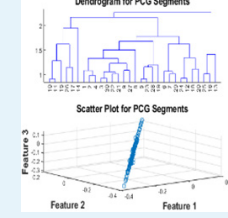
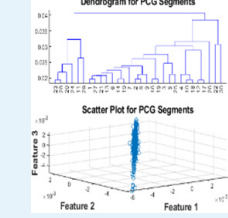
Process/Samples	ECG-1	ECG-2	PCG-1	PCG-2
Input				
Denosing				
Peak detection				
Dendrogram with scatter plot				

Table 1 Illustrates the image results of the proposed work according to input, denoising, peak detection, and dendrogram with a scatter plot.

### 4.2 Peak optimization performance

Table 2 shows the performance of different models regarding peak localization. To find the performance, various metrics are used: mean absolute error (MAE), mean absolute percentage error (MAPE), mean squared error (MSE), root mean squared Error (RMSE), peak signal-to-noise ratio (PSNR), and localization error (LE). In Table 2, we can see the performance of the proposed DCWT has the highest PSNR

value, i.e., (32.3258 dB), which explains that it is producing the best quality signals or images compared to other models such as DWT, stationary wavelet transform (SWT), continuous wavelet transform (CWT) and lifting wavelet transform (LWT). Hence, the proposed DCWT outperforms other methods.

**Table 2.** Performance of peak optimization

Peak Localization	MAE	MAPE	MSE	RMSE	PSNR (db)	Localization Error
<b>Proposed DCWT</b>	2.1845	1.9645	1.7865	1.3218	32.3258	4.89
<b>Existing DWT</b>	3.2875	2.1956	2.1054	1.8961	20.4556	6.87
<b>Existing SWT</b>	7.4354	6.3912	4.8568	2.5461	16.1747	8.65
<b>Existing CWT</b>	9.5932	8.7854	7.8245	6.4541	13.7945	9.45
<b>Existing LWT</b>	10.8475	9.7595	8.7745	7.1257	12.4478	10.11

## 5 DISCUSSIONS

### 5.1 Performance analysis

Figure 3 illustrates the performance analysis of the proposed FEDRIS and traditional techniques such as FIS, sigmoid fuzzy logic (SFL), trapezoidal fuzzy logic (TFL), and decision rule (DR) regarding rule generation time (RGT), fuzzification time (FT), and defuzzification time (DT). The proposed method introduces the EDR membership function to elevate the prediction outcomes. The proposed FEDRIS acquired an RGT, FT, and DT of 496ms, 633ms, and 631ms, respectively. However, the existing methods obtained an average RGT, FT, and DT of 650ms, 840ms, and 841ms, correspondingly. Thus, the proposed technique had impressive results.

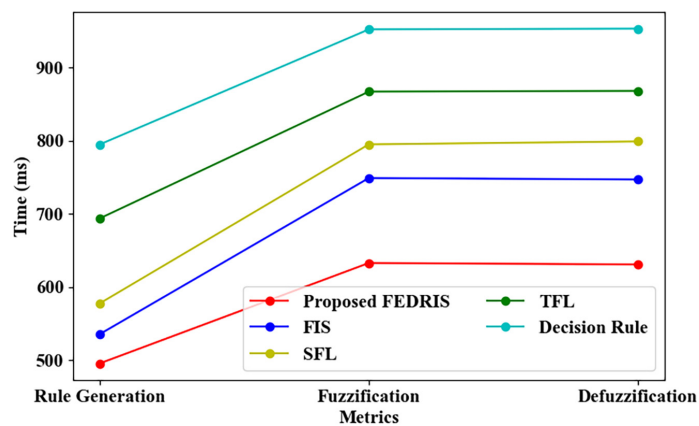


**Fig. 3.** Performance assessment of the proposed approach

The performance assessment of the proposed DGMC-L<sub>1,2</sub> and existing techniques such as DCNN, deep neural network (DNN), recurrent neural network (RNN), and artificial neural network (ANN) is represented in Figure 4. The proposed DGMC-L<sub>1,2</sub> achieved an accuracy, precision, recall, and f-measure of 98.997%, 98.993%, 98.998%, and 98.975, respectively. Likewise, the traditional classifiers attained average accuracy, precision, recall, and f-measure of 91.746%, 91.210%, 92.146%, and 91.553%, respectively. Thus, the proposed methodology had higher significance.

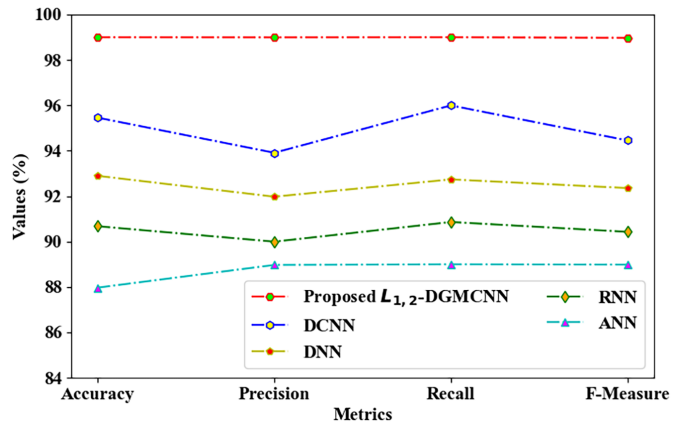


Fig. 4. Performance analysis

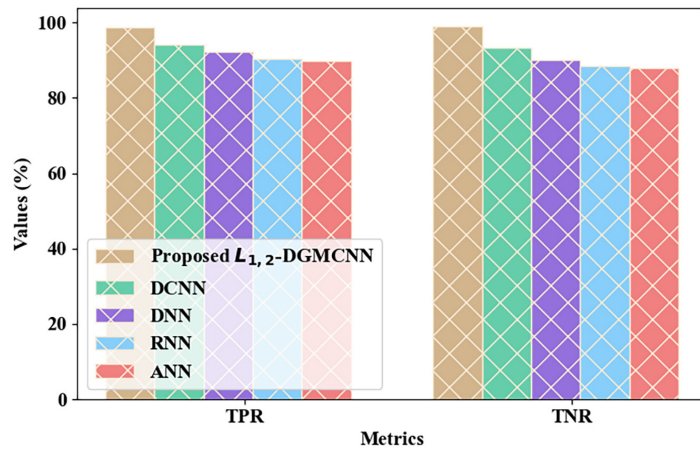


Fig. 5. TPR and TNR assessment

In Figures 5 and 6, the performance of the proposed DGMC- $L_{1,2}$  is analyzed by comparing it with associated classifiers based on true positive rate (TPR), true negative rate (TNR), false positive rate (FPR), and false negative rate (FNR). The proposed DGMC- $L_{1,2}$  attained a TPR, TNR, FPR, and FNR of 98.77%, 98.88%, 0.312, and 0.203, respectively. Yet, the traditional classifiers had fewer outcomes. Hence, the proposed method has proved to be a less error-prone model.

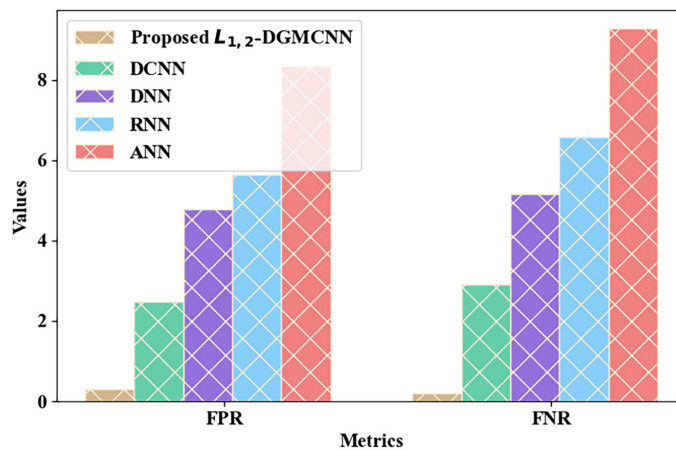


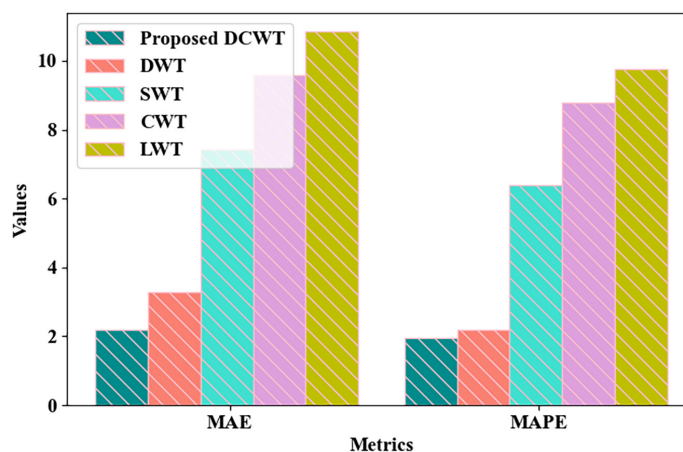
Fig. 6. FPR and FNR validation

**Table 3.** Training time validation

Techniques	Training Time (ms)
Proposed DGMC-L <sub>1,2</sub>	45687
DCNN	51699
DNN	59479
RNN	63296
ANN	79645

Table 3 validates the training time (TT) of the proposed DGMC-L<sub>1,2</sub> and existing techniques. The proposed DGMC-L<sub>1,2</sub> takes a minimum TT of 45687ms, whereas the traditional approaches obtained an average TT of 63529ms. Therefore, the research methodology had low time complexity.

Figure 7 demonstrates the performance validation of the proposed DCWT and traditional techniques such as DWT, SWT, CWT, and LWT regarding MAE and MAPE. The cross-entropy decomposition is introduced to upgrade the model's accuracy. The proposed DCWT obtained an MAE and MAPE of 2.18 and 1.96, respectively. However, the traditional approaches had maximum error values. Hence, the proposed approach outperforms the prevailing techniques.

**Fig. 7.** MAE and MAPE evaluation**Table 4.** Localization error

Technique	Localization Error
Proposed DCWT	4.89
DWT	6.87
SWT	8.65
CWT	9.45
LWT	10.11

The LE of the proposed DCWT and traditional techniques is analyzed in Table 4. The proposed DCWT attained a LE of 4.89, whereas the conventional algorithms acquired an average LE of 8.77. Therefore, the proposed work had more accurate results.

## 5.2 Comparative analysis

The reliability of the proposed work is validated by comparing it with related works.

**Table 5.** Comparative evaluation

Reference	Techniques	Accuracy (%)	Precision (%)
The proposed system	DGMC-L <sub>1,2</sub>	98.99	98.99
[16]	SVM	90.9	88.0
[17]	Deep-CNN	97.0	97.0
[18]	SVM	87.3	–
[19]	KNN	94	88.0
[20]	CNN	90.43	93.67

Table 5 compares the proposed system and existing works. The proposed DGMC-L<sub>1,2</sub> establishes the L<sub>1,2</sub> norm-regularization and GM activation functions to improve learning efficiency. The proposed DGMC-L<sub>1,2</sub> obtained an accuracy and precision of 98.99% and 98.99%, respectively. Furthermore, the existing methodologies establish techniques such as SVM, Deep-CNN, and KNN. Yet, the traditional approaches had limited outcomes owing to the ineffective hyperparameter selection. The proposed work had superior performance.

## 6 CONCLUSION

This paper proposed a leading framework named DGMC-L<sub>1,2</sub>-based multi-heart disease prediction using ECG and PCG. The proposed DGMC-L<sub>1,2</sub> efficiently classifies the various types of HD, increasing the patient's survival time. Thus, the experimental outcomes showed that the proposed DGMC-L<sub>1,2</sub> attained an accuracy, precision, TPR, and FPR of 98.99%, 98.99%, 98.77%, and 0.312, respectively, depicting the model's reliability. Similarly, the proposed FEDRIS obtained an RGT and FT of 496ms and 633ms, respectively, showing the low time complexity. Thus, the research methodology aids in improving the therapeutic measures of HD patients.

## 7 ACKNOWLEDGMENT

The resources and computing environment were provided by the VNRVJIET. We are thankful for their support.

## 8 REFERENCES

- [1] I. M. El-Hasnony, O. M. Elzeki, A. Alshehri, and H. Salem, "Multi-label active learning-based machine learning model for heart disease prediction," *Sensors*, vol. 22, no. 3, p. 1184, 2022. <https://doi.org/10.3390/s22031184>
- [2] W. Chen, Q. Sun, X. Chen, G. Xie, H. Wu, and C. Xu, "Deep learning methods for heart sounds classification: A systematic review," *Entropy*, vol. 23, no. 6, p. 667, 2021. <https://doi.org/10.3390/e23060667>



- [3] M. Alkhodari and L. Fraiwan, "Convolutional and recurrent neural networks for the detection of valvular heart diseases in phonocardiogram recordings," *Computer Methods and Programs in Biomedicine*, vol. 200, p. 105940, 2021. <https://doi.org/10.1016/j.cmpb.2021.105940>
- [4] M. N. M. Nawi, M. F. Omar, R. A. Odeh, A. G. Hanafi, F. A. A. Nifa, and M. K. I. A. Rahim, "A conceptual approach of an integrated multi criteria decision making techniques and deep learning for construction project managers selection problem," *International Journal of Interactive Mobile Technologies (ijIM)*, vol. 18, no. 13, pp. 166–178, 2024. <https://doi.org/10.3991/ijim.v18i13.49119>
- [5] B. J. Sowmya *et al.*, "A visual computing unified application using deep learning and computer vision techniques," *International Journal of Interactive Mobile Technologies (ijIM)*, vol. 18, no. 1, pp. 59–74, 2024. <https://doi.org/10.3991/ijim.v18i01.42673>
- [6] P. Li, Y. Hu, and Z.-P. Liu, "Prediction of cardiovascular diseases by integrating multi-modal features with machine learning methods," *Biomedical Signal Processing and Control*, vol. 66, p. 102474, 2021. <https://doi.org/10.1016/j.bspc.2021.102474>
- [7] R. Hettiarachchi *et al.*, "A novel transfer learning-based approach for screening pre-existing heart diseases using synchronized ECG signals and heart sounds," in *2021 IEEE International Symposium on Circuits and Systems (ISCAS)*, Daegu, Korea, 2021, pp. 1–5. <https://doi.org/10.1109/ISCAS51556.2021.9401093>
- [8] S. Tiwari, A. Jain, A. K. Sharma, and K. Mohamad Almustafa, "Phonocardiogram signal based multi-class cardiac diagnostic decision support system," *IEEE Access*, vol. 9, pp. 110710–110722, 2021. <https://doi.org/10.1109/ACCESS.2021.3103316>
- [9] S. Aziz, M. U. Khan, M. Alhaisoni, T. Akram, and M. Altaf, "Phonocardiogram signal processing for automatic diagnosis of congenital heart disorders through fusion of temporal and cepstral features," *Sensors*, vol. 20, no. 13, p. 3790, 2020. <https://doi.org/10.3390/s20133790>
- [10] S. S. Kumar and K. Vijayalakshmi, "Coronary artery disease detection from PCG signals using time domain based automutual information and spectral features," in *2020 International Conference on Computing, Electronics & Communications Engineering (iCCECE)*, Southend, UK, 2020, pp. 69–74. <https://doi.org/10.1109/iCCECE49321.2020.9231107>
- [11] M. Boulares, R. Alotaibi, A. AlMansour, and A. Barnawi, "Cardiovascular disease recognition based on heartbeat segmentation and selection process," *International Journal of Environmental Research and Public Health*, vol. 18, no. 20, p. 10952, 2021. <https://doi.org/10.3390/ijerph182010952>
- [12] B. Kumar, R. Soundararajan, K. Natesan, and R. M. Santhi, "Hybrid feature selection and classifying stages through electrocardiogram (ECG) signal for heart disease prediction," *Eng. Proc.*, vol. 59, no. 1, p. 126, 2023. <https://doi.org/10.3390/engproc2023059126>
- [13] T. Tuncer, S. Dogan, R.-S. Tan, and U. R. Acharya, "Application of Petersen graph pattern technique for automated detection of heart valve diseases with PCG signals," *Information Sciences*, vol. 565, pp. 91–104, 2021. <https://doi.org/10.1016/j.ins.2021.01.088>
- [14] M. U. Khan, S. Aziz, K. Iqtidar, G. F. Zaher, S. Alghamdi, and M. Gull, "A two-stage classification model integrating feature fusion for coronary artery disease detection and classification," *Multimedia Tools and Applications*, vol. 81, no. 10, pp. 13661–13690, 2021. <https://doi.org/10.1007/s11042-021-10805-3>
- [15] S. K. Ghosh, R. N. Ponnalagu, R. K. Tripathy, and U. R. Acharya, "Automated detection of heart valve diseases using chirplet transform and multiclass composite classifier with PCG signals," *Computers in Biology and Medicine*, vol. 118, p. 103632, 2020. <https://doi.org/10.1016/j.compbiomed.2020.103632>

- [16] T. Liu *et al.*, “Detection of coronary artery disease using multi-domain feature fusion of multi-channel heart sound signals,” *Entropy*, vol. 23, no. 6, p. 642, 2021. <https://doi.org/10.3390/e23060642>
- [17] A. Mehmood *et al.*, “Prediction of heart disease using deep convolutional neural networks,” *Arabian Journal for Science and Engineering*, vol. 46, no. 4, pp. 3409–3422, 2021. <https://doi.org/10.1007/s13369-020-05105-1>
- [18] S. B. Shuvo, S. N. Ali, S. I. Swapnil, M. S. Al-Rakhami, and A. Gumaei, “CardioXNet: A novel lightweight deep learning framework for cardiovascular disease classification using heart sound recordings,” *IEEE Access*, vol. 9, pp. 36955–36967, 2021. <https://doi.org/10.1109/ACCESS.2021.3063129>
- [19] U. Riaz, S. Aziz, M. Umar Khan, S. A. A. Zaidi, M. Ukasha, and A. Rashid, “A novel embedded system design for the detection and classification of cardiac disorders,” *Computational Intelligence*, vol. 37, no. 4, pp. 1844–1864, 2021. <https://doi.org/10.1111/coin.12469>
- [20] H. Li *et al.*, “A fusion framework based on multi-domain features and deep learning features of phonocardiogram for coronary artery disease detection,” *Computers in Biology and Medicine*, vol. 120, p. 103733, 2020. <https://doi.org/10.1016/j.compbiomed.2020.103733>

## 9 AUTHORS

**Dakshayani Himabindu Damineni** received her B.Tech degree in information technology from JNTUH University, Hyderabad, India, in 2006 and her M.Tech degree in information technology from IARE, JNTUH University, Hyderabad, India. Currently working as an assistant professor in the IT department at VNR Vignana Jyothi Institute of Engineering and Technology, Hyderabad, India. Since 2019, Pursuing PhD from GITAM (Deemed to be University), Vizag, India. Her research interests are deep learning, machine learning, AI, and cloud computing. She has lifetime membership in the international association of Engineers (IAENG) (E-mail: [dakshayani.himabindu@gmail.com](mailto:dakshayani.himabindu@gmail.com)).

**CH. Srilakshmi** is working as an Assistant Professor in the CSE-IOT Department, CBIT. She has 10 years of experience. Her areas of interest include deep learning, machine learning and computer vision. Currently pursuing PhD in JNTUK (E-mail: [chsrilu.45@gmail.com](mailto:chsrilu.45@gmail.com)).

**Jakkula Sravanthi** received her B.Tech degree in Computer Science Engineering from JITS, Karimnagar, affiliated to JNTUH University, Hyderabad, India 2013 and M.Tech degree in Computer Networks & Information Security from JITS, Karimnagar, affiliated to JNTUH University, Hyderabad, India 2015. Currently, she is working as an Assistant Professor, IT Department in VNR Vignana Jyothi Institute of Engineering and Technology, Hyderabad, India. Since 2022, Pursuing Ph.D from NIT, Warangal, India. Her research interests lies in Bioinformatics, Deep learning, Machine Learning (E-mail: [sravs521@gmail.com](mailto:sravs521@gmail.com)).

**Dr. B. Sivalakshmi** was awarded Ph.D from Acharya Nagarjuna University. She is currently working as an Associate Professor and HOD in the Department of Information Technology and MCA. Her areas of research interest include Image processing, AI, Machine learning and Deep learning. She has fourteen years of teaching and research experience and is a member of four professional organizations. She has 10 Scopus indexed publications, 10 NPTEL certifications, and one book chapter to her credit.

**Satish Kumar Mirtipati** received his MCA degree in Information Technology from JNTU-GV University, Vizianagaram, India 2023. Currently, he is working as

an Assistant Professor, CSE Department in Centurion University of Technology and Management, Andhra Pradesh, India, since 2023. His research interests lies in Computer Networking, Internet of Things, Deep learning, Machine Learning, AI, and Cloud Computing. He is one of the committee member in BoS of JNTU-GV (E-mail: [satishkumarsrk@icloud.com](mailto:satishkumarsrk@icloud.com)).

**Prasanthi Yavanamandha**, a research scholar in the Department of Computer Science and Engineering at Koneru Lakshmaiah Deemed to be University in Hyderabad, India. She hold a Bachelor's Degree in Information Technology, which is completed in 2007, and a Master's Degree in Software Engineering, which is obtained in 2011. Currently, she is working as an Assistant Professor, CSE-AIML & IOT Deaprtment VNR Vignana Jyothi Institute of Engineering and Technology, Hyderabad, India. Her research interests lie in the areas of Deep Learning, Data Science, and Machine Learning.